Published in final edited form as:
Neuron. 2013 August 21; 79(4): 738–753. doi:10.1016/j.neuron.2013.06.012.

Interaural Level Difference Dependent Gain Control and Synaptic Scaling Underlying Binaural Computation

Xiaorui R. Xiong[1,2,*], **Feixue Liang**[5,*], **Haifu Li**[5], **Lukas Mesik**[1,2], **Ke K. Zhang**[7], **Daniel B. Polley**[6], **Huizhong W. Tao**[1,4], **Zhongju Xiao**[5,#], and **Li I. Zhang**[1,3,#]

[1]Zilkha Neurogenetic Institute, Keck School of Medicine, University of Southern California, Los Angeles, 90033, USA

[2]Neuroscience Graduate Program, Keck School of Medicine, University of Southern California, Los Angeles, 90033, USA

[3]Department of Physiology and Biophysics, Keck School of Medicine, University of Southern California, Los Angeles, 90033, USA

[4]Department of Cell and Neurobiology, Keck School of Medicine, University of Southern California, Los Angeles, 90033, USA

[5]Department of Physiology, School of Basic Medical Sciences, Southern Medical University, Guangzhou 510515, China

[6]Eaton-Peabody Laboratories, Massachusetts Eye and Ear Infirmary and Department of Otology and Laryngology, Harvard Medical School, Boston MA 02114, USA

[7]Department of Pathology, University of North Dakota, Grand Forks, ND 58202, USA

Abstract

Binaural integration in the central nucleus of inferior colliculus (ICC) plays a critical role in sound localization. However, its arithmetic nature and underlying synaptic mechanisms remain unclear. Here, we showed in mouse ICC neurons that the contralateral dominance is created by a "push-pull"-like mechanism, with contralaterally dominant excitation and more bilaterally balanced inhibition. Importantly, binaural spiking response is generated apparently from an ipsilaterally-mediated scaling of contralateral response, leaving frequency tuning unchanged. This scaling effect is attributed to a divisive attenuation of contralaterally-evoked synaptic excitation onto ICC neurons with their inhibition largely unaffected. Thus, a gain control mediates the linear transformation from monaural to binaural spike responses. The gain value is modulated by interaural level difference (ILD) primarily through scaling excitation to different levels. The ILD-dependent synaptic scaling and gain adjustment allow ICC neurons to dynamically encode interaural sound localization cues while maintaining an invariant representation of other independent sound attributes.

[#]Correspondence should be addressed to: L.I. Zhang (liizhang@usc.edu) or Z. Xiao (xiaozj@fimmu.com).
[*]These authors contribute equally to this study.

Introduction

The central nucleus of the inferior colliculus (ICC) is a critical center for binaural processing. In addition to intracollicular synaptic inputs, ICC neurons receive ascending inputs from nearly all auditory brainstem nuclei (Casseday et al., 2002; Grothe et al., 2010; Pollak, 2012). By integrating contralaterally and ipsilaterally evoked inputs, ICC neurons can perform multiple functional tasks in parallel: the processing of sound attributes per se, such as frequency and intensity, and the processing of binaural sound localization cues such as interaural time and level differences (ITD and ILD, respectively). Despite many previous studies, the arithmetic nature of binaural integration, viz., the transfer function between monaural and binaural spike responses, remains not well defined. Most binaural studies have focused on neural tuning for the spatial location of sound sources, or have varied the acoustic parameters that contribute most to sound localization (Chase and Young, 2005; Delgutte et al., 1999; Irvine and Gago, 1990; Kelly and Phillips, 1991; Kuwada et al., 1987; Semple and Kitzes, 1985; Wenstrup et al., 1988). In this study, we reveal the monaural-to-binaural spike response transformation by examining the complete auditory receptive fields under contralateral, ipsilateral, and binaural stimulation conditions.

Most ICC neurons are driven strongly by contralateral sound sources, due to the major contralateral excitatory projections from cochlear nuclei and lateral superior olive (LSO) (Adams, 1979; Brunso-Bechtold et al., 1981; Ross and Pollak, 1989). Ipsilaterally presented sound can suppress, have no effect on, or in some cases enhance the binaural spike response relative to the response driven contralaterally alone (Irvine and Gago, 1990; Roth et al., 1978; Semple and Aitkin, 1979; Wenstrup et al., 1988). These interaural interactions can potentially be described with three simple arithmetic forms when the generation of binaural frequency tuning is considered (Figure 1A; Experimental Procedures): 1) a summation or subtraction between contralateral and ipsilateral spike responses; 2) a thresholding effect on the contralateral spike response, with the ipsilateral input serving to increase or decrease the effective spike threshold; and 3) a multiplicative or divisive normalization (i.e. gain modulation) of the contralateral spike response. These three types of response transformation will have different impacts on auditory processing. Both the summation/subtraction and thresholding effects would change the spectral processing by altering the sharpness of frequency tuning, whereas the gain modulation effect preserves the frequency tuning regardless of changes in spike rate. In addition, from the transfer function between contralateral and binaural spike responses, we can clearly define the role of ipsilateral input in binaural processing. To determine the transfer function underlying the binaural processing of spectral information, we compared the frequency-intensity tonal receptive fields (TRFs) of spike responses driven monaurally and binaurally. We found in both anaesthetized and awake mice that binaural responses resulted from a scaling of contralateral responses, with ipsilateral input serving as a gain control. In addition, we provided evidence that the gain value was modulated by ILD. Thus, it can potentially be employed to represent sound source location.

For a thorough understanding of the monaural-to-binaural spike response transformation, it is essential to reveal the underlying synaptic mechanisms with intracellular recordings. Since the output response is primarily determined by the excitatory and inhibitory synaptic interplay, the potential modulations of binaural spike response could be due to changes in excitatory input, inhibitory input, or a combination of both. A small number of intracellular studies (Covey et al., 1996; Kuwada et al., 1997; Li et al., 2010; Nelson and Erulkar, 1963; Peterson et al., 2008) reported membrane potential responses evoked by contralateral, ipsilateral and binaural stimulation, based on which potential circuit interactions have been proposed. However, due to the difficulty in deriving the absolute levels of excitation and inhibition from the recorded membrane potential responses, the excitatory and inhibitory

synaptic mechanisms for binaural integration remain unclear. In this study, we applied *in vivo* whole-cell voltage-clamp recordings to dissect the contralaterally, ipsilaterally and binaurally evoked excitatory and inhibitory synaptic inputs. Our results indicated that the ipsilateral input mediated gain modulation was achieved primarily through an ILD-dependent scaling of excitatory synaptic input.

Results

Monaural frequency representation of mouse ICC neurons

We first characterized the monaural frequency representation of mouse ICC neurons by presenting sound to the contralateral and ipsilateral ears separately (see Experimental Procedures). *In vivo* loose-patch cell-attached recordings were made from ICC neurons to examine their spike responses to tone pips of different frequencies and intensities presented to the contralateral or ipsilateral ear in a random sequence (see Experimental Procedures). Spike TRFs were reconstructed from responses to contralateral and ipsilateral stimuli (Figure 1B). The contralateral TRF was not only broader than the ipsilateral TRF, but also had a lower intensity threshold and higher spike rates. Thus, the cell showed a contralateral bias. To quantify the monaurality of ICC neurons, we used an aural dominance index (ADI), which was defined as the difference between contralateral and ipsilateral responses summed across the entire TRF, divided by their sum ((Contra−Ipsi)/(Contra+Ipsi)). A total of 105 ICC neurons were recorded. Among these cells, 33% (35 out of 105) exhibited spiking responses to contralateral stimuli only, resulting in an ADI of 1 (Figure 1C). The rest of the neurons exhibited both contralateral and ipsilateral spike responses, but the contralateral response was stronger than the ipsilateral response, as indicated by the result that all ADI values were positive (Figure 1C). This result is consistent with previous observations in various species that most of ICC neurons are more strongly driven by contralaterally presented sound (Kelly et al., 1991; Kuwada et al., 1997; Popescu and Polley, 2010; Semple and Aitkin, 1979). In our recorded ICC neurons, a great majority had an ADI higher than 0.5 (Figure 1C) and a broader contralateral TRF than the ipsilateral counterpart (Figure 1D), indicating a strong contralateral bias in the mouse ICC. For cells that had both contralateral and ipsilateral TRFs, the ipsilateral intensity threshold was usually higher than the contralateral threshold (Figure 1E), and the onset latency of the ipsilateral response was usually longer than that of the contralateral response (Figure 1F). Despite these differences, contralateral and ipsilateral TRFs displayed about the same characteristic frequency (CF) (Figure 1G), indicating a matched tonotopic map between contralateral and ipsilateral stimulation (Popescu and Polley, 2010). In a few cells, spontaneous membrane rupture occurred, allowing us to record spike and subthreshold responses simultaneously. As shown in an example monaural cell (Figure 1H), ipsilateral stimulation clearly evoked synaptic responses, although only spike responses to contralateral stimulation were observed. This observation is consistent with reports of previous intracellular studies (Kuwada et al., 1997; Li et al., 2010), indicating that monaural cells can in fact receive binaural synaptic inputs and that spike threshold has greatly enhanced the monaurality of output responses (Liu et al., 2010; Priebe, 2008).

Synaptic inputs underlying the contralateral aural dominance

To further examine the synaptic inputs underlying contralaterally and ipsilaterally evoked spike responses, we made whole-cell voltage-clamp recordings from ICC neurons (see Experimental Procedures). Excitatory and inhibitory synaptic currents were dissected by clamping the cell's membrane potential at −70 mV and 0 mV respectively. From the example cell shown in Figure 2A, three salient properties of synaptic inputs were observed. First, the contralateral excitatory input was stronger than the ipsilateral counterpart. This contralateral bias of excitatory input likely underlies the aural preference of most ICC

neurons (Figure 1C). Second, the inhibitory TRF was much broader than its excitatory counterpart, and this is the case for both contralateral and ipsilateral stimulation. That inhibition is broader than excitation is consistent with a recent report in the rat IC (Kuo and Wu, 2012). Third, the difference between amplitudes of contralateral and ipsilateral synaptic responses was less striking for inhibition compared to excitation.

We recorded from eighteen ICC neurons. One cell did not show ipsilaterally evoked excitatory or inhibitory responses (i.e. purely monaural). The rest displayed both contralaterally and ipsilaterally evoked synaptic responses. In 14 of these neurons, a complete set of excitatory and inhibitory synaptic TRFs to both contralateral and ipsilateral stimulation were obtained. We summarized the amplitude relationship between the contralateral and ipsilateral responses taken around the best frequency and at 70 dB sound pressure level (SPL). The contralateral bias of synaptic amplitude was significantly greater for excitation than for inhibition as measured by ADI (Figure 2B) and contralateral-ipsilateral difference (Figure S1A). Notably the average ADI of inhibition was much closer to zero compared to excitation, indicating that inhibitory responses were more binaurally balanced. Due to the differential aural dominance of excitation and inhibition, the excitation/inhibition (E/I) ratio was significantly lower for ipsilateral than contralateral stimulation (Figure 2C). Therefore, the stronger contralateral excitation and relatively stronger ipsilateral inhibition (analogous to a “push-pull” pattern) can both contribute to the contralateral dominance of ICC spiking responses. Finally, we summarized the bandwidths of contralateral and ipsilateral synaptic TRFs (Figure 2D). For both excitation and inhibition, the contralateral TRF was broader than the ipsilateral counterpart. In addition, the inhibitory TRF was broader than the corresponding excitatory TRF, for both contralateral and ipsilateral stimulation (Figure 2D). Such broad inhibition may contribute to the inhibitory sidebands revealed by the effects of GABAergic manipulations on extracellularly recorded unit spikes (Vater et al., 1992; Yang et al., 1992). The contralateral and ipsilateral synaptic TRFs had the same CF, and the excitatory and inhibitory TRFs for the same ear stimulation also exhibited the same CF (Figure S1B–S1D).

A linear transformation of the contralateral into binaural spike response

We next examined how monaural spike responses are transformed into a binaural spike response. By presenting the same set of tones contralaterally, ipsilaterally and binaurally in a random order, we reconstructed three spike TRFs for each recorded cell. As a starting point, we set the binaural stimuli to have the same intensity at both ears (i.e. ILD = 0 dB), which mimics the ILD for a sound source originated on the midline. As shown by an example cell (Figure 3A), the binaural TRF clearly resembled the contralateral TRF, whereas the ipsilateral TRF appeared much smaller. To quantify the relationship between the binaural and contralateral TRFs, we plotted the binaural response level against the corresponding contralateral spike response level (Figure 3B). It became clear that the binaural responses linearly correlated with the contralateral responses, with a correlation coefficient (r) as high as 0.96 (Figure 3B, whole). The binaural spike response was suppressed relative to the contralateral spike response, as evidenced by the < 1 slope of the linear fitting, indicating that the cell was an EI neuron (e.g. the influence of ipsilateral input is inhibitory) (Irvine and Gago, 1990; Kelly et al., 1991; Kuwada et al., 1997; Semple and Kitzes, 1985; Wenstrup et al., 1988). Interestingly, the slope of linear fitting was almost the same when only the responses within the effective frequency-intensity region where there were no ipsilateral spiking responses were considered (Figure 3B, w/o ipsi). Collectively, these results suggest that despite the frank spike response evoked by the ipsilateral ear input alone, its primary contribution to binaural tuning is to modulate the contralateral response. More example cells are shown in Figure S2A–S2D.

We found a strong linear correlation between the levels of binaural and contralateral spike responses in all the neurons examined, with their correlation coefficients all ≥ 0.8 (Figure 3C, black). In contrast, the correlation between binaural and ipsilateral spike responses was much weaker (Figure 3C, red). This result suggests that the binaural spike response can be viewed as being scaled from the contralateral spike response, with the scaling factor (i.e. slope/gain) controlled by the ipsilateral ear input. Figure 3D shows the distribution of gain values for monaural cells (i.e. cells that do not show ipsilateral spike responses, red) and binaural cells (calculated for responses in the entire TRF, black). The distribution was similar for monaural and binaural neurons. For binaural neurons, no correlation was observed between gain value and the relative strength of ipsilateral spike response (Figure 3D, inset). These results suggest that the gain modulation effect was independent of presence of ipsilateral spike responses. For the majority of cells, the gain was lower than 1, consistent with previous observations that EI neurons are the largest population in the ICC (Casseday et al., 2002; Grothe et al., 2010; Pollak, 2012). For the binaural neurons, we further compared the gain values calculated for responses in the entire effective frequency-intensity space, and those in TRF regions without displaying ipsilateral spike responses. As shown in Figure 3E, gain values measured in the two ways were similar to each other, again supporting the notion that ipsilateral ear input plays a modulatory role. To assess the statistical accuracy of the measured gain value, we applied bootstrap method (Carandini et al., 1997; Efron and Tibshirani, 1993) for each cell. The measured gain value matched closely to the mean of bootstrapped gain values, deviating from it by no more than 2% (Figure S2E–S2G). In addition, the variation of bootstrapped gain values was small, mostly less than 10% (Figure S2H). This analysis supports the statistical accuracy of the measured gain values. Consistent with the notion of a scaling of contralateral spike responses, the binaural TRF exhibited the same CF (Figure 3F) and a similar bandwidth (Figure 3G) as that of the contralateral TRF. With multiple linear regression (see Experimental Procedures), we statistically determined on a single-cell basis that there was no significant contribution ($p > 0.05$) from the ipsilateral spike response to the binaural spike response in 123 out of 131 recorded neurons (104 from anaesthetized, and 27 from awake animals) and that there was no significant thresholding effect ($p > 0.05$; see Experimental Procedures) in 127 out of 131 neurons (the p values for the other cells are larger than 0.01). In contrast, the contralateral response was found to be highly significantly correlated with the binaural response ($p < 10^{-15}$) in all the 131 neurons. Together, these results further suggest that binaural spike responses can be best described as a scaling up/down of contralateral spike responses, with the ipsilateral ear input providing the gain control.

Synaptic mechanisms for the gain control effect

How is the ipsilateral input-mediated gain control achieved? To further understand binaural integration at the synaptic level, we recorded excitatory and inhibitory synaptic TRFs to both monaural and binaural stimulation. As shown by an example cell in Figure 4A, the cell received stronger excitatory inputs driven contralaterally than ipsilaterally, while its inhibitory inputs driven contralaterally and ipsilaterally in large part had similar amplitudes. From the synaptic amplitudes, it is clear that the binaural synaptic response was neither a subtraction nor a summation between the contralateral and ipsilateral responses. Similar to the analysis of spiking responses, we plotted the binaural synaptic amplitude against the contralateral synaptic amplitude to the same tone stimulus (Figure 4B). The correlation coefficient was high for both the excitatory and inhibitory synaptic responses, indicating a strong linear relationship. The slope of linear fitting was 0.81 for excitation, but 0.98 for inhibition. This indicates that the binaural excitatory input was significantly scaled down from the contralateral excitatory input, whereas the binaural inhibitory input was not very different from its contralateral counterpart. A second example cell is shown in Figure S3A–S3B.

As summarized for 11 similarly recorded cells, the linear correlation between binaural and contralateral synaptic responses was strong, with the *r* mostly larger than 0.8 for both excitation and inhibition (Figure 4C). On average, the contralateral excitatory synaptic response (measured around the best frequency and at 70 dB SPL) was stronger than the binaural excitatory response ($p < 0.01$, paired t-test), while the contralateral inhibitory synaptic response was not different from its binaural counterpart ($p > 0.2$, paired t-test) (Figure 4D). In contrast, ipsilateral excitatory and inhibitory inputs were both weaker than their binaural counterparts ($p < 0.01$, paired t-test), but the difference was far smaller for inhibition than excitation (Figure 4D). Figure 4E plots the scaling factor for the contralateral-to-binaural synaptic response transformation. In all the recorded cells, the scaling factor for excitation was below 1, indicating a suppressive effect despite the fact that ipsilateral stimulation alone evoked excitation. The scaling factor for inhibition was close to 1, indicating a much weaker modulation of inhibition by ipsilateral stimulation. As for receptive field shape, binaural synaptic TRFs closely resembled their contralateral counterparts, as demonstrated by their similar bandwidths (Figure 4F) and CFs (Figure S3C–S3D). On the other hand, ipsilateral synaptic TRFs were significantly narrower than their binaural counterparts (Figure 4F). Together, these summaries strengthen the notion that ipsilateral ear input serves a modulatory function in generating binaural spike responses primarily by scaling down contralaterally evoked excitatory input.

To test whether the observed scaling of excitatory input contributes to the apparent linear transformation of the contralateral into binaural spike response, we employed a conductance-based neuron model (Liu et al., 2011; Zhou et al., 2012). Figure 5A and 5B show the tone-evoked excitatory and inhibitory synaptic inputs at 70 dB SPL for a typical ICC neuron. We fit the frequency distribution of synaptic response amplitudes with a Gaussian function (Figure 5C and 5D). The normalized Gaussian functions for binaural and contralateral synaptic responses superimposed well (Figure 5C and 5D, inset), indicating little difference in tuning shape and again supporting the notion of scaling. We utilized these Gaussian fits to simulate frequency tuning of excitatory and inhibitory synaptic inputs in our model. For simplicity, the best frequencies of excitation and inhibition were chosen to be the same (see Figure S3C–S3D), and their tuning shapes were both symmetric (Figure 5E). Tone-evoked excitatory and inhibitory conductances (Figure 5E, inset) were simulated by fitting experimental data with an alpha function (see Experimental Procedures). Each tone-evoked membrane potential (Vm) response was then derived by integrating the corresponding excitatory and inhibitory conductances in the neuron model (see Experimental Procedures), with their amplitudes varied at different tone frequencies according to their corresponding frequency tuning curves. We scaled the excitatory synaptic amplitude by a factor of 0.8 – 1.2, while kept the inhibitory response amplitude unchanged (see Figure 4E). Figure 5F shows the frequency tuning curves of peak Vm responses at different excitatory scaling factors. To derive spiking response from the peak Vm response, we utilized a power-law function in describing the relation between Vm and spike rate (Atallah et al., 2012; Liu et al., 2011; Miller and Troyer, 2002; Priebe, 2008) (see Experimental Procedures). As shown in Figure 5G, the scaling of excitatory response amplitudes resulted in negligible changes in the shape of spike tuning, although the spike rate could be modulated by as much as 50%. Within the experimentally observed range of changes of spike rate (0.4 – 1.4 fold, see Figure 1D), excitation was scaled within a range of 0.78 – 1.12 fold, and spike tuning width only varied between a narrow range of 0.93 – 1.03 fold (Figure 5H). Similar as previously reported (Atallah et al., 2012), scaling of inhibition can also achieve an approximate gain control of spike responses (Figure 5I). The gain modulation by scaling excitation was not affected much by the inhibitory tuning shape, as similar effects on spike tuning were achieved under inhibition cotuned with excitation, more broadly tuned than excitation, or inhibition with a flat tuning (Figure 5J).

The gain value is modulated by interaural level difference

Previous studies have demonstrated that the amplitude of binaural spike response can be modulated by interaural level/intensity difference (ILD), a spatial location cue (Irvine and Gago, 1990; Kuwada et al., 1997; Li et al., 2010; Pollak, 2012; Semple and Kitzes, 1985; Wenstrup et al., 1988). In the experiments described thus far, ILD was set as zero to simulate a sound source originating on the auditory midline. To test whether a linear transformation of the contralateral into binaural spike response also applies to other binaural hearing conditions, we varied ILD to simulate different sound source locations. As shown by an example cell in Figure 6A, the binaural TRFs at several different ILDs all resembled the TRF under contralateral stimulation alone. At each ILD tested, a strong linear correlation between binaural and contralateral spike responses was observed (Figure 6B, 6C). Noticeably, the gain value decreased as ILD became increasingly ipsilaterally dominant, suggesting the progressively increasing influence of ipsilaterally-mediated suppression at more ipsilaterally dominant ILDs (Figure 6C). In a total of 24 similarly recorded neurons, except for two cells exhibiting enhancement, the majority of cells showed a reduction of binaural spike response with decreasing ILD (Figure 6C). The linear correlation between binaural and contralateral spike responses was similarly strong (r close to 1) at all testing ILDs and in all the cells examined (Figure 6E), indicating that gain modulation is a general phenomenon. We measured the rate of modulation between 0 and −20 dB ILD (Figure 6F). The gain value is modulated roughly monotonically by ILD. There was no significant correlation between the gain value (at −20 dB ILD) and the CF of the recorded cell (Figure 6G). Finally, for every ILD tested, the binaural TRF resembled the contralateral TRF, as reflected by their similar CFs, 20 dB bandwidths and intensity thresholds (Figure 6H–J).

Synaptic mechanisms underlying the ILD-dependent gain modulation

We further examined synaptic changes underlying the ILD-dependent gain modulation. We recorded binaurally evoked excitation and inhibition to CF tones while varying ILD. The binaural synaptic responses were compared to the response evoked by contralateral stimulation alone. As shown by an example cell in Figure 7A, as ILD became increasingly ipsilaterally dominant, the excitatory synaptic response was gradually reduced in amplitude, while the inhibitory synaptic response was not apparently changed (Figure 7B). This trend was observed in 7 similarly recorded cells (Figure 7C, 7D). From the summary of modulation rate, calculated as the percentage difference of the binaural response at the lowest ILD tested compared to that at the highest ILD tested (Figure 7E), we concluded that binaurally evoked synaptic excitation was significantly reduced at more ipsilaterally dominant ILDs, whereas synaptic inhibition was not significantly affected by varying ILD. Thus, the ILD-dependent gain modulation is primarily achieved by modulating excitatory input amplitude.

Binaural integration in awake conditions

Does the linear transformation of the contralateral into binaural spike response observed in anesthetized animals also occur in awake conditions? To address this issue, we developed a head-fixed awake recording system (Figure 8A) and carried out loose-patch recordings. As shown by an example cell in Figure 8B, the spike TRFs recorded in the awake ICC were well-tuned and V-shaped, similar to those from anesthetized animals. The contralateral TRF was stronger than the ipsilateral TRF, and the binaural TRF resembled the contralateral TRF. Similar to the anesthetized condition, the binaural spike response (at ILD = 0 dB) linearly correlated with the contralateral response (Figure 8C). In all the 27 cells successfully recorded, the linear correlation between binaural and contralateral spike responses was strong, as evidenced by the r higher than 0.8 (Figure 8D). The distribution of gain values of these cells (Figure 8E) was also consistent with that under anesthesia, with the majority of cells exhibiting a suppressive gain. In a subset of cells, we varied ILD. As

shown by an example cell in Figure 8F, the binaural TRFs with different ILDs all resembled the contralateral TRF. The gain value decreased with decreasing ILD, while the linear correlation between binaural and contralateral spike responses remained as strong (Figure 8F, 8G). In the recorded population, all neurons except two exhibited an ILD-dependent increase in suppressive gain (Figure 8H). In all the neurons, the r remained close to 1 across different testing ILDs (Figure 8I). Similar as inan aesthetized conditions, the binaural TRF resembled the contralateral TRF at every ILD tested, in terms of CF, bandwidth and intensity threshold (Figure 8J–8L). Altogether, our data demonstrate that ipsilaterally-mediated gain modulation does prevail in awake conditions.

Discussion

In this study, we systematically investigated several fundamental aspects of binaural processing in the mouse ICC: 1) the synaptic mechanisms for the contralateral dominance of ICC spike responses; 2) the arithmetic function for the transformation of monaural into binaural spike responses; 3) the synaptic mechanisms underlying this transformation; 4) the modulation of the monaural-to-binaural spike response transformation by ILD. By examining binaural and monaural spike responses to a broad variety of tone stimuli, our study, for the first time, proposes a gain control mechanism for binaural integration, i.e. binaural spike response results from a scaling of the contralateral spike response, with the ipsilateral ear input functioning as the gain modulation. With *in vivo* whole-cell voltage-clamp recordings, we further concluded that the ipsilaterally-mediated gain control is mainly achieved through a scaling of contralaterally evoked excitatory inputs, with inhibitory inputs relatively constant under monaural and binaural hearing conditions. In addition, we showed that the gain value is modulated by ILD, a spatial localization cue for high-frequency sound, and that the modulation is primarily achieved through an ILD-dependent scaling of excitatory input.

An inhibitory mechanism contributes to contralateral aural dominance

Most cells in the ICC respond more strongly to sounds in the contralateral field. This can be attributed to a crossed pattern of major excitatory pathways to the ICC, e.g. LSO and CN projections from the contralateral side (Casseday et al., 2002). Although the difference between excitation driven by contralateral and ipsilateral projections can directly lead to a contralateral preference, our study reveals that an inhibitory mechanism also contributes significantly to the contralateral aural dominance. Instead of exhibiting a similar contralateral dominance, inhibitory inputs to the ICC are more binaurally balanced in terms of synaptic amplitude, with a significantly lower ADI than excitation. This may reflect the diverse feedforward inhibitory projections that impinge upon the ICC. For example, ICC receives inhibition bilaterally from the dorsal nucleus of lateral lemniscus (DNLL), in addition to inhibition from LSO neurons on the same side and IC neurons on the opposite side (Casseday et al., 2002; Helfert and Aschoff, 1997; Moore et al., 1998). The contralaterally stronger excitation and bilaterally more balanced inhibition results in a larger E/I ratio for the contralaterally-driven input, which would further enhance the difference between contralateral and ipsilateral spiking responses under the spike thresholding effect (Liu et al., 2010; Priebe, 2008). The sharp difference in binaurality between the excitation and inhibition to ICC neurons is consistent with the distinct crossed and uncrossed pathways of excitatory and inhibitory projections.

Differential binaural integration of excitation and inhibition

The ICC receives innervations from almost all the lower brainstem auditory nuclei, some of which are monaural while others are binaural (Kudo and Nakamura, 1987; Pollak and Casseday, 1989; Helfert and Aschoff, 1997; Casseday et al., 2002; Grothe et al., 2010;

Pollak, 2012). Parsing the unique contribution of each feedforward circuit to binaural processing in the ICC remains a major challenge. In this study, the revealed monaural-to-binaural spike response transformation and its synaptic underpinning may illuminate the principal anatomical determinants of complex signal integration in the ascending projections to the ICC neurons. Here, we propose the most parsimonious explanation for the observed binaural integration of excitatory input, based on the current understanding of auditory brainstem circuits. In all the recorded cells, the binaurally evoke excitatory current was much smaller than the summation of ipsilaterally and contralaterally evoked excitatory currents. In addition, the gain value does not correlate with the strength of ipsilateral response. These findings directly demonstrate that at least some binaural interactions are shaped within the brainstem, and are preserved in the afferent input to the ICC neurons reported here. As reported in previous studies, the superior olivary complex is the first stage to extract detailed information relating interaural time and level differences (Casseday et al., 2002; Kavanagh and Kelly, 1992; Moore and Caspary, 1983). The fact that binaurally evoked excitation is weaker than that obtained with contralateral stimulation alone can likely be attributed a fundamental transformation of the afferent signal provided by feedforward inhibition from the medial nucleus of the trapezoid body (MNTB) onto LSO neurons (Cant and Casseday, 1986; Casseday et al., 2002; Moore and Caspary, 1983; Pollak, 2012). MINTB inhibition may also be responsible for the nearly complete silencing of ipsilateral excitatory inputs generated by MSO and LSO neurons, thereby scaling down the contralateral excitatory input under binaural stimulation conditions. Thus, the apparent gain modulation of spike responses of ICC neurons may largely reflect a decoding of the binaural computation performed in binaural nuclei prior to the ICC (e.g. LSO). However, it is worth noting that ICC neurons also receive excitatory input from other sources under binaural stimulation, e.g. monaural inputs (both contralateral and ipsilateral; e.g. Li and Pollak, 2013) and the top-down modulatory inputs. Due to these additional inputs, it is possible that ICC neurons can perform additional binaural computation.

Compared to excitation, inhibition to most ICC neurons is relatively unchanged by binaural stimulation. This again may be attributed to more or less balanced inhibitory projections from contralateral and ipsilateral sides. The origins of these projections are mostly binaural nuclei (e.g. DNLL, LSO, ICC), with most of their neurons exhibiting EI properties (Casseday et al., 2002). Perhaps under binaural hearing conditions at 0 dB ILD, projections representing each side are both suppressed equally, resulting in a summed inhibitory current relatively unchanged compared to the currents evoked unilaterally. It is worth noting that the small decrease in inhibition by binaural stimulation observed in some cells (Figure 4E) may underlie the facilitative binaural interaction occurring in a small portion of ICC neurons (see Figure 3D). Compared to excitatory pathways, the current understanding of inhibitory circuits is more limited (Casseday et al., 2005). The potential circuitry mechanism underlying the complex signal integration in the ICC remains to be explored in future experiments.

Ipsilaterally-mediated ILD-dependent gain modulation

By varying the ILD of CF tones or noise, the sensitivity to ILD of ICC neurons has been characterized extensively (e.g. Irvine and Gago, 1990; Semple and Kitzes, 1987). In this study, the application of a broad variety of tone stimuli allowed us to more definitively determine the role of ipsilateral input in binaural integration under different hearing conditions. The ipsilateral input provides a gain modulation of the contralateral input.. This is further evidenced by the result that the same gain value was obtained in different regions of the binaural receptive field. For most of ICC neurons, the gain value decreases as ILD becomes increasingly ipsilaterally dominant, consistent with the reported property of EI cells (Irvine and Gago, 1990; Kuwada et al., 1997; Li et al., 2010; Pollak, 2012; Semple and

Kitzes, 1985; Wenstrup et al., 1988). Interestingly, the gain value is modulated by ILD in a relatively linear manner, and the rate of gain change is specific to individual cells. These observations raise a hypothesis that the azimuthal location of sound sources is encoded by the gain in individual ICC neurons, and that higher order neurons can extract this information based on the population activity of these cells.

Our whole-cell recording data suggest that the modulation of gain by ILD is achieved primarily through modifying the excitatory input amplitude, whereas the inhibitory input amplitude remains relatively constant across different ILDs. This difference again may be explained by the more balanced contralateral and ipsilateral projections for inhibitory input and the binaural properties of inhibitory neuron sources. Perhaps as sound source becomes more peripheral, inhibition from contralateral and ipsilateral sources exhibits symmetric changes in the opposite directions, result in a largely unchanged summed inhibitory current.

Gain control and parallel processing

Gain control is known to play a critical role in many aspects of sensory processing (Salinas and Sejnowski, 2001). For example, a gain modulation allows invariant tuning properties regardless of changes in stimulus intensity (Atallah et al., 2012; Olsen et al., 2012; Rabinowitz et al., 2011). Recently, it has been reported in the mouse visual cortex that changing the activity level of specific inhibitory neurons results in an approximate scaling up/down of orientation tuning curves of excitatory neurons with negligible changes in tuning width (Atallah et al., 2012; Lee et al., 2012; Olsen et al., 2012; Wilson et al., 2012). In principle, modulating either excitatory or inhibitory synaptic input may produce a gain change (Chance et al., 2002). Our experimental data and modeling results demonstrate that scaling excitation alone can result in an approximate gain modulation of spike responses. For auditory processing, gain modulation in the monaural-to-binaural spike response transformation provides a foundation for preserving the representation of location-independent acoustic attributes (e.g. sound frequency) in individual cells under monaural and binaural hearing conditions. This is likely a general multiplexing strategy for neurons to simultaneously extract, transform, and transmit multiple embedded stimulus attributes.

Experimental Procedures

Anaesthetized animal preparation and sound stimulation

All experimental procedures used in this study were approved by the Animal Care and Use Committee of the University of Southern California and Southern Medical University of China. Experiments were carried out in a sound attenuation booth. Female adult mice (12 – 16 weeks, C57BL/6) were sedated with chlorprothixene (0.05 ml of 4 mg/ml) and anesthetized with urethane (1.2 g/kg). Heart beat rate, respiration rate, and body temperature were monitored throughout each experiment. Body temperature was maintained at 37.5°C using a homoeothermic system (Harvard Instruments). After opening the right part of occipital bone above the IC, the dura was removed. The IC surface was covered with an artificial cerebrospinal fluid (ACSF; in mM: 124 NaCl, 1.2 NaH_2PO4, 2.5 KCl, 25 $NaHCO_3$, 20 Glucose, 2 $CaCl_2$, 1 $MgCl_2$). Tone pips (50 ms duration, 3 ms ramp) of various frequencies (2–32 kHz, at 0.1 octave interval) and intensities (0–70 sound pressure level, at 10 dB interval) were presented to the contralateral, ipsilateral ear separately or simultaneously to both ears in a randomized sequence via a calibrated closed acoustic delivery system comprising of two TDT EC1 speakers with couplers. By monitoring extracellular responses in the cochlear nucleus, we found that the interaural attenuation was > 45 dB for all test frequencies. Sound was generated with custom softwares (LabView, National Instrument) controlled by a National Instrument interface. The IC area was first mapped by recording multiunit spikes with a parylene-coated tungsten electrode (2 MΩ,

FHC), which were evoked by contralateral stimulation only. Electrode signals were amplified and band-pass filtered between 300 and 6000 Hz (Plexon). A customized LabView software was used for data acquisition and pre-processing such as on-line extracting of spike times and plotting of receptive fields. The ICC region was identified based on short response latencies (6–10 ms for noise response), sharply tuned tonal receptive fields as well as a dorsal-to-ventral gradient of characteristic frequency (from low to high) (Stiebler and Ehret, 1985; Willott, 1984; Yu et al., 2005).

In vivo whole-cell and loose-patch recordings

Whole-cell and loose-patch recordings were performed with an Axopatch 200B amplifier (Molecular Devices), as previously described (Sun et al., 2010; Wu et al., 2008; Zhou et al., 2010). The patch pipette (Kimax) had a tip opening of about 1.5 μm (4–6 MΩ). For whole-cell recording, the intrapipette solution contained (in mM): 125 Cs-gluconate, 5 TEA-Cl, 4 MgATP, 0.3 GTP, 8 phosphocreatine, 10 HEPES, 10 EGTA, 2 CsCl, 1 QX-314, 0.75 MK-801, 1% biocytin (pH 7.25). The pipette capacitance and whole-cell capacitance were compensated completely, and the series resistance (20–40 MΩ) was compensated by 50% – 60% (at 100 μs lag). An estimated junction potential of 11 mV was corrected. Only neurons with relatively stable series resistance (< 15% change during the recording) were used for further analysis. Histology was performed as previously described (Wu et al., 2008; Zhou et al., 2010). For loose-patch recordings, glass electrodes with the same opening size containing a K^+-based solution (130 K-gluconate, 2 KCl, 1 $CaCl_2$, 10 HEPES, 11 EGTA, pH 7.25) were used.

Data analysis

Tone evoked responses—Spike TRFs were mapped for at least 10 repetitions, and synaptic TRFs were mapped for 2–3 repetitions. Tone-driven spikes were counted within a 0–60 ms time window after the tone onset. The average number of evoked spikes for each tone was used for plotting the spike TRF. The boundaries of spike TRFs were defined with a custom-written software in MATLab, following previous descriptions (Sutter and Schreiner, 1991; Schumacher, et al. 2011). The spike response latency was defined as the lag between the stimulus onset and the negative peak of the first evoked spike. Synaptic response traces evoked by the same test stimuli were averaged, and the onset latency was identified at the time point in the rising phase of the response waveform, where the amplitude exceeded the baseline current by two standard deviations. Only excitatory responses with an onset latency of 5–15 ms were considered in this study. For each cell, bootstrap sampling (*bootstrp*, MATLab, 1000 times) was applied to determine the statistics of the gain value.

Synaptic conductances—Excitatory and inhibitory synaptic conductances were derived (Anderson et al., 2000; Borg-Graham et al., 1998; Sun et al., 2010; Wu et al., 2008; Zhou et al., 2010) according to $\Delta I = Ge*(V-Ee) + Gi*(V-Ei)$. ΔI is the amplitude of the synaptic current at any time point after subtracting of the baseline current; Ge and Gi are the excitatory and inhibitory synaptic conductance; V is the holding voltage, and Ee (0 mV) and Ei (−70mV) are the reversal potentials. The clamping voltage V was corrected from the applied holding voltage (Vh): $V = Vh - Rs*I$, where Rs is the effective series resistance. By holding the recorded cell at two different voltages (the reversal potentials for excitatory and inhibitory current respectively), Ge and Gi could be resolved from the equation.

Modeling—The synaptic inputs to a pyramidal neuron in ICC were simulated by the following equation (Zhou et al., 2012):

$$G_e(t)=a \cdot H(t-t_0) \cdot (1-e^{-(t-t_0)/\tau_{rise}}) \cdot e^{-(t-t_0)/\tau_{decay}}$$
$$G_i(t)=b \cdot H(t-t_0) \cdot (1-e^{-(t-t_0)/\tau_{rise}}) \cdot e^{-(t-t_0)/\tau_{decay}}$$

$G_e(t)$ and $G_i(t)$ are the modeled synaptic conductances; a and b are the amplitude factors. a is a Gaussian function with sigma = 0.5 octave and b is a Gaussian with sigma =1 octave. $H(t)$ is the Heaviside step function; t_0 is the onset delay of synaptic input. τ_{rise} and τ_{decay} define the shape of the rising phase and decay of the synaptic current. The values for τ_{rise} and τ_{decay} were chosen by fitting the average shape of the recorded synaptic responses with the above function. The onset difference between excitatory and inhibitory conductances was set as 2 ms based on our experimental observation. Membrane potential was derived from the simulated synaptic conductances based on an integrate-and-fire model:

$$V_m(t+dt)=-\frac{dt}{C}[G_e(t)*(V_m(t)-E_e)+G_i(t)*(V_m(t)-E_i)+G_r(V_m(t)-E_r)]+V_m(t)$$

where $V_m(t)$ is the membrane potential at time t, C the whole-cell capacitance, G_r the resting leakage conductance, E_r the resting membrane potential (−65 mV). C was measured during experiments and G_r was calculated based on the equation $G_r = C*G_m/C_m$, where G_m, the specific membrane conductance is $2e^{-5}$ S/cm^2, and C_m, the specific membrane capacitance is $1e^{-6}$ F/cm^2 (Hines, 1993; Stuart and Nelson, 1998). A power-law spike thresholding scheme (Liu et al., 2011; Miller and Troy, 2002)was applied as:

$$R(V_m)=k[V_m-V_{rest}]_+^P$$

R is the firing rate, k is the gain factor (set as 9e5 to obtain experimentally observed firing rates), p (=3) is the exponent. The "+" indicates rectification, i.e. the values below zero are set as zero. Varying the p value from 2 to 5 did not qualitatively change our conclusion.

Arithmetic functions and multiple linear regression—Three arithmetic transformation functions examined in this study were: 1) a summation/subtraction between ipsilateral and contralateral responses ($R_{bi} = R_{contra} +/- R_{ipsi}$); 2) a thresholding of the contralateral response ($R_{bi} = R_{contra} +/- k$); 3) a multiplicative scaling of the contralateral response ($R_{bi} = k * R_{contra}$). Multiple linear regression was applied to model the relationship between the binaural response (R_{bi}) and the contra- and ipsi-lateral responses (R_{contra} and R_{ipsi}, respectively). The recorded spike responses in the TRF of each neuron were fit with the following function: $R_{bi} = \alpha * R_{contra} + \beta * R_{ipsi} + \gamma$. The p values for each variable for each neuron were corrected with Bonferroni correction for multiple tests. Statistical tests indicated that neither R_{ipsi} nor γ contributed significantly to R_{bi}, and that a multiplicative scaling best described the data.

Awake animal preparation—One week before recording, mice were anaesthetized with 1.5% isoflurane. The scalp was removed. A screw was mounted on the skull with dental cement. Animals were injected subcutaneously with 0.1mg/kg buprenorphine and put back in the home cage to recover. During the recovery period, mice were trained to be accustomed to the head fixation on the recording setup. To fix the head, the screw was tightly clamped onto a metal post. The animal was able to run freely on a plastic plate rotating around its center as described in a recent study (Olsen et al., 2012). On the day of recording, surgery was performed in the sound-attenuation booth. Mice were anaesthetized with 1.5% isoflurane. The head was fixed to the metal post. A craniotomy over the IC was

made. The dura was removed. The animal was allowed to recover from isoflurane for at least 30 minutes. Recording was started after the animal exhibited normal running. The recording session lasted for about 2–4 hours. The animal was given drops of 5% glucose through a pipette every hour.

Supplementary Material

Refer to Web version on PubMed Central for supplementary material.

Acknowledgments

This work was supported by grants to L.I.Z. from the US National Institutes of Health (NIH; R01DC008983), and the David and Lucile Packard Foundation (Packard Fellowships for Science and Engineering). H.W.T. was supported by an NIH grant R01EY019049. D.B.P was supported byan NIH grant R01DC009836. K.K.Z was supported by NIH grants P20RR016471, and P20GM103442. Z.X., L.Z., F.L. was supported by China NSF grants (31228013, 31171059, 31200831) and a research program IRT1142 in China.

References

Adams JC. Ascending projections to the inferior colliculus. J Comp Neurol. 1979; 183:519–538. [PubMed: 759446]

Anderson JS, Carandini M, Ferster D. Orientation tuning of input conductance, excitation, and inhibition in cat primary visual cortex. J Neurophysiol. 2000; 84:909–926. [PubMed: 10938316]

Atallah BV, Bruns W, Carandini M, Scanziani M. Parvalbumin-expressing interneurons linearly transform cortical responses to visual stimuli. Neuron. 2012; 73:159–170. [PubMed: 22243754]

Borg-Graham LJ, Monier C, Fregnac Y. Visual input evokes transient and strong shunting inhibition in visual cortical neurons. Nature. 1998; 393:369–373. [PubMed: 9620800]

Brunso-Bechtold JK, Thompson GC, Masterton RB. HRP study of the organization of auditory afferents ascending to central nucleus of inferior colliculus in cat. J Comp Neurol. 1981; 197:705–722. [PubMed: 7229134]

Cant NB, Casseday JH. Projections from the anteroventral cochlear nucleus to the lateral and medial superior olivary nuclei. J Comp Neurol. 1986; 247:457–476. [PubMed: 3722446]

Carandini M, Heeger DJ, Movshon JA. Linearity and normalization in simple cells of the macaque primary visual cortex. J Neurosci. 1997; 17:8621–8644. [PubMed: 9334433]

Casseday, JH.; Fremouw, T.; Covey, E. The inferior colliculus: a hub for the central auditory system. In: Oertel, D.; Popper, AN.; Fay, RR., editors. Integrative Functions in the Mammalian Auditory Pathway. New York: Springer-Verlag; 2002. p. 238-318.

Casseday, JH.; Schreiner, CE.; Winer, JA. The Inferior Colliculus: Past, Present, and Future. In: WJA; SCE, editors. The Inferior Colliculus. New York: Springer Inc; 2005. p. 312-345.

Chance FS, Abbott LF, Reyes AD. Gain modulation from background synaptic input. Neuron. 2002; 35:773–782. [PubMed: 12194875]

Chase SM, Young ED. Limited segregation of different types of sound localization information among classes of units in the inferior colliculus. J Neurosci. 2005; 25:7575–7585. [PubMed: 16107645]

Covey E, Kauer JA, Casseday JH. Whole-cell patch-clamp recording reveals subthreshold sound-evoked postsynaptic currents in the inferior colliculus of awake bats. J Neurosci. 1996; 16:3009–3018. [PubMed: 8622130]

Delgutte B, Joris PX, Litovsky RY, Yin TC. Receptive fields and binaural interactions for virtual-space stimuli in the cat inferior colliculus. J Neurophysiol. 1999; 81:2833–2851. [PubMed: 10368401]

Efron, B.; Tibshirani, R. An introduction to the bootstrap. New York: Chapman & Hall; 1993.

Grothe B, Pecka M, McAlpine D. Mechanisms of sound localization in mammals. Physiol Rev. 2010; 90:983–1012. [PubMed: 20664077]

Helfert, RH.; Aschoff, A. Superior olivary complex and nuclei of the lateral lemniscus. In: EG; RR, editors. The Central Auditory System. New York: Oxford University Press; 1997. p. 193-258.

Hines, M. Neural Systems: Analysis and Modeling. MA: Kluwer academic; 1993. NEURON–a program for simulation of nerve equations.

Irvine DR, Gago G. Binaural interaction in high-frequency neurons in inferior colliculus of the cat: effects of variations in sound pressure level on sensitivity to interaural intensity differences. J Neurophysiol. 1990; 63:570–591. [PubMed: 2329362]

Kavanagh GL, Kelly JB. Midline and lateral field sound localization in the ferret (Mustela putorius): contribution of the superior olivary complex. J Neurophysiol. 1992; 67:1643–1658. [PubMed: 1629768]

Kelly JB, Glenn SL, Beaver CJ. Sound frequency and binaural response properties of single neurons in rat inferior colliculus. Hear Res. 1991; 56:273–280. [PubMed: 1769920]

Kelly JB, Phillips DP. Coding of interaural time differences of transients in auditory cortex of Rattus norvegicus: implications for the evolution of mammalian sound localization. Hear Res. 1991; 55:39–44. [PubMed: 1752792]

Kudo, M.; Nakamura, K. Organization of the lateral lemniscal fibers converging onto the inferior colliculus in the cat: an anatomical review. In: SJ; MRB, editors. Auditory Pathway: Structure and Function. New York: Plenum Press; 1987. p. 171-183.

Kuo RI, Wu GK. The generation of direction selectivity in the auditory system. Neuron. 2012; 73:1016–1027. [PubMed: 22405210]

Kuwada S, Batra R, Yin TC, Oliver DL, Haberly LB, Stanford TR. Intracellular recordings in response to monaural and binaural stimulation of neurons in the inferior colliculus of the cat. J Neurosci. 1997; 17:7565–7581. [PubMed: 9295401]

Kuwada S, Stanford TR, Batra R. Interaural phase-sensitive units in the inferior colliculus of the unanesthetized rabbit: effects of changing frequency. J Neurophysiol. 1987; 57:1338–1360. [PubMed: 3585471]

Lee SH, Kwan AC, Zhang S, Phoumthipphavong V, Flannery JG, Masmanidis SC, Taniguchi H, Huang ZJ, Zhang F, Boyden ES, Deisseroth K, Dan Y. Activation of specific interneurons improves V1 feature selectivity and visual perception. Nature. 2012; 488:379–383. [PubMed: 22878719]

Li N, Gittelman JX, Pollak GD. Intracellular recordings reveal novel features of neurons that code interaural intensity disparities in the inferior colliculus. J Neurosci. 2010; 30:14573–14584. [PubMed: 20980615]

Li N, Pollak GD. Circuits that innervate excitatory-inhibitory cells in the inferior colliculus obtained with in vivo whole cell recordings. J Neurosci. 2013; 33:6367–6379. [PubMed: 23575835]

Liu BH, Li P, Sun YJ, Li YT, Zhang LI, Tao HW. Intervening inhibition underlies simple-cell receptive field structure in visual cortex. Nat Neurosci. 2010; 13:89–96. [PubMed: 19946318]

Liu BH, Li YT, Ma WP, Pan CJ, Zhang LI, Tao HW. Broad inhibition sharpens orientation selectivity by expanding input dynamic range in mouse simple cells. Neuron. 2011; 71:542–554. [PubMed: 21835349]

Miller KD, Troyer TW. Neural noise can explain expansive, power-law nonlinearities in neural response functions. J Neurophysiol. 2002; 87:653–659. [PubMed: 11826034]

Moore DR, Kotak VC, Sanes DH. Commissural and lemniscal synaptic input to the gerbil inferior colliculus. J Neurophysiol. 1998; 80:2229–2236. [PubMed: 9819238]

Moore MJ, Caspary DM. Strychnine blocks binaural inhibition in lateral superior olivary neurons. J Neurosci. 1983; 3:237–242. [PubMed: 6822858]

Nelson PG, Erulkar SD. Synaptic Mechanisms of Excitation and Inhibition in the Central Auditory Pathway. J Neurophysiol. 1963; 26:908–923. [PubMed: 14084166]

Oliver DL, Kuwada S, Yin TC, Haberly LB, Henkel CK. Dendritic and axonal morphology of HRP-injected neurons in the inferior colliculus of the cat. J Comp Neurol. 1991; 303:75–100. [PubMed: 2005240]

Olsen SR, Bortone DS, Adesnik H, Scanziani M. Gain control by layer six in cortical circuits of vision. Nature. 2012; 483:47–52. [PubMed: 22367547]

Peterson DC, Voytenko S, Gans D, Galazyuk A, Wenstrup J. Intracellular recordings from combination-sensitive neurons in the inferior colliculus. J Neurophysiol. 2008; 100:629–645. [PubMed: 18497365]

Pollak GD. Circuits for processing dynamic interaural intensity disparities in the inferior colliculus. Hear Res. 2012; 288:47–57. [PubMed: 22343068]

Pollak, GD.; Casseday, JH. The Neural Basis of Echolocation in Bats. New York: Springer-Verlag; 1989.

Popescu MV, Polley DB. Monaural deprivation disrupts development of binaural selectivity in auditory midbrain and cortex. Neuron. 2010; 65:718–731. [PubMed: 20223206]

Priebe NJ. The relationship between subthreshold and suprathreshold ocular dominance in cat primary visual cortex. J Neurosci. 2008; 28:8553–8559. [PubMed: 18716214]

Rabinowitz NC, Willmore BD, Schnupp JW, King AJ. Contrast gain control in auditory cortex. Neuron. 2011; 70:1178–1191. [PubMed: 21689603]

Ross LS, Pollak GD. Differential ascending projections to aural regions in the 60 kHz contour of the mustache bat's inferior colliculus. J Neurosci. 1989; 9:2819–2834. [PubMed: 2549219]

Roth GL, Aitkin LM, Andersen RA, Merzenich MM. Some features of the spatial organization of the central nucleus of the inferior colliculus of the cat. J Comp Neurol. 1978; 182:661–680. [PubMed: 721973]

Salinas E, Sejnowski TJ. Gain modulation in the central nervous system: where behavior, neurophysiology, and computation meet. Neuroscientist. 2001; 7:430–440. [PubMed: 11597102]

Schumacher JW, Schneider DM, Woolley SM. Anesthetic state modulates excitability but not spectral tuning or neural discrimination in single auditory midbrain neurons. J Neurophysiol. 2011; 106:500–514. [PubMed: 21543752]

Semple MN, Aitkin LM. Representation of sound frequency and laterality by units in central nucleus of cat inferior colliculus. J Neurophysiol. 1979; 42:1626–1639. [PubMed: 501392]

Semple MN, Kitzes LM. Single-unit responses in the inferior colliculus: different consequences of contralateral and ipsilateral auditory stimulation. J Neurophysiol. 1985; 53:1467–1482. [PubMed: 4009228]

Semple MN, Kitzes LM. Binaural processing of sound pressure level in the inferior colliculus. J Neurophysiol. 1987; 57:1130–1147. [PubMed: 3585457]

Stiebler I, Ehret G. Inferior colliculus of the house mouse. I A quantitative study of tonotopic organization, frequency representation, and tone-threshold distribution. J Comp Neurol. 1985; 238:65–76. [PubMed: 4044904]

Stuart G, Spruston N. Determinants of voltage attenuation in neocortical pyramidal neuron dendrites. J Neurosci. 1998; 18:3501–3510. [PubMed: 9570781]

Sun YJ, Wu GK, Liu BH, Li P, Zhou M, Xiao Z, Tao HW, Zhang LI. Fine-tuning of pre-balanced excitation and inhibition during auditory cortical development. Nature. 2010; 465:927–931. [PubMed: 20559386]

Sutter ML, Schreiner CE. Physiology and topography of neurons with multipeaked tuning curves in cat primary auditory cortex. J Neurophysiol. 1991; 65:1207–1226. [PubMed: 1869913]

Vater M, Habbicht H, Kossl M, Grothe B. The functional role of GABA and glycine in monaural and binaural processing in the inferior colliculus of horseshoe bats. J Comp Physiol. 1992; 171:541–553. [PubMed: 1469669]

Wenstrup JJ, Fuzessery ZM, Pollak GD. Binaural neurons in the mustache bat's inferior colliculus. I Responses of 60-kHz EI units to dichotic sound stimulation. J Neurophysiol. 1988; 60:1369–1383. [PubMed: 3193162]

Willott JF. Changes in frequency representation in the auditory system of mice with age-related hearing impairment. Brain Res. 1984; 309:159–162. [PubMed: 6488006]

Wilson NR, Runyan CA, Wang FL, Sur M. Division and subtraction by distinct cortical inhibitory networks in vivo. Nature. 2012; 488:343–348. [PubMed: 22878717]

Wu GK, Arbuckle R, Liu BH, Tao HW, Zhang LI. Lateral sharpening of cortical frequency tuning by approximately balanced inhibition. Neuron. 2008; 58:132–143. [PubMed: 18400169]

Yang L, Pollak GD, Resler C. GABAergic circuits sharpen tuning curves and modify response properties in the mustache bat inferior colliculus. J Neurophysiol. 1992; 68:1760–1774. [PubMed: 1479443]

Yu X, Wadghiri YZ, Sanes DH, Turnbull DH. In vivo auditory brain mapping in mice with Mn-enhanced MRI. Nat Neurosci. 2005; 8:961–968. [PubMed: 15924136]

Zhou Y, Liu BH, Wu GK, Kim YJ, Xiao Z, Tao HW, Zhang LI. Preceding inhibition silences layer 6 neurons in auditory cortex. Neuron. 2010; 65:706–717. [PubMed: 20223205]

Zhou Y, Mesik L, Sun YJ, Liang F, Xiao Z, Tao HW, Zhang LI. Generation of spike latency tuning by thalamocortical circuits in auditory cortex. J Neurosci. 2012; 32:9969–9980. [PubMed: 22815511]

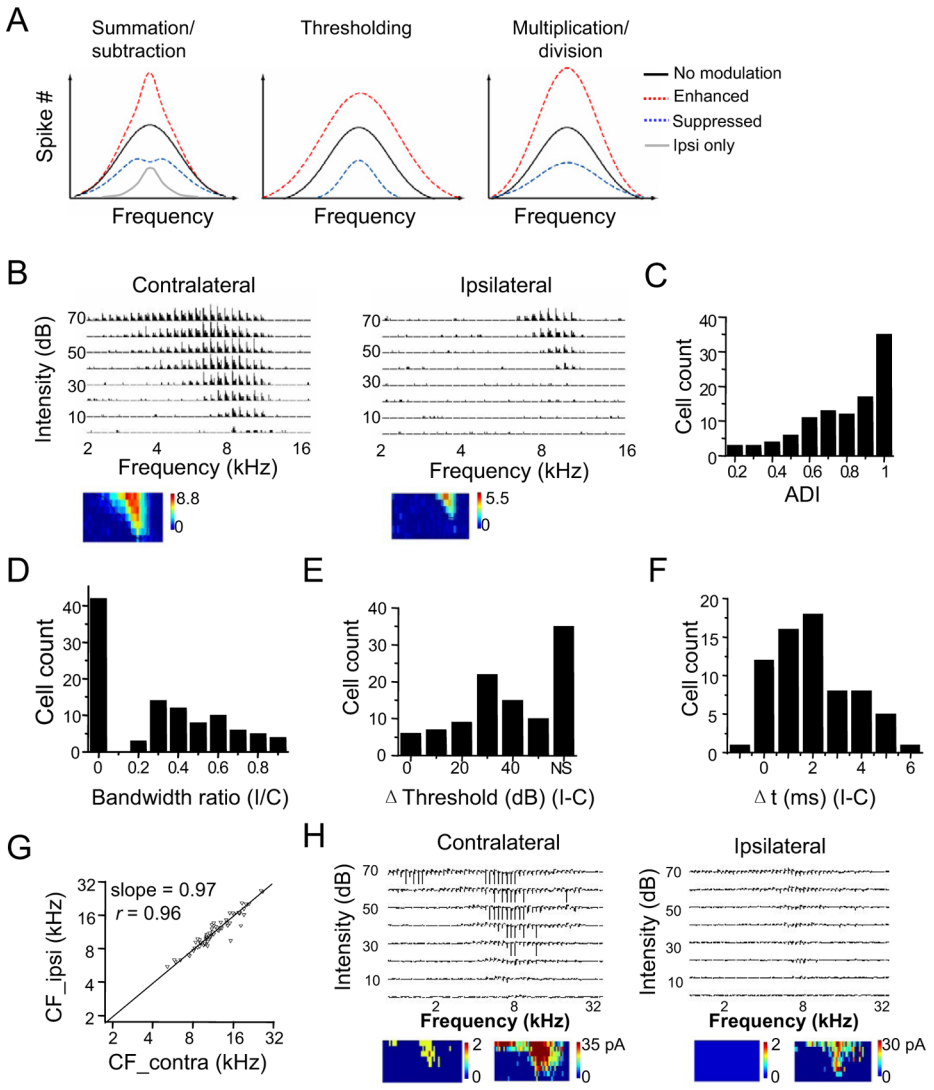

Figure 1. Monaural frequency representation of mouse ICC neurons

(A) Three potential forms of binaural interaction. Curves shown are schematic frequency tuning curves of binaural response (spike) resulting from a summation/subtraction between ipsilateral and contralateral responses, from a thresholding effect on the contralateral response, as well as from a multiplicative scaling of the contralateral response. Black curve: binaural tuning equivalent to contralateral tuning alone. Gray curve: ipsilateral tuning alone.

(B) Spike TRFs of an example ICC neuron driven by tones presented to the contralateral and ipsilateral ear respectively. Each small trace represents a post-stimulus spike time histogram (PSTH, 10 trials) for recorded spikes within 50 ms after the tone onset, at a given frequency-intensity combination. The color map below depicts the average spike number per trial within the 50 ms window.

(C) Distribution of the aural dominance index (ADI). Cells with ADI = 1 only exhibit contralaterally evoked spike responses.

(D) Distribution of the ratio between monaural TRF bandwidths (ipsi/contra).

(E) Distribution of the intensity threshold difference between monaural TRFs (ipsi-contra). “NS” represents cells that did not show ipsilaterally evoked spike responses.

(F) Distribution of the difference between response onset latencies (ipsi-contra), measured around the best frequency and at 70 dB sound pressure level (SPL). Monaural cells are excluded.
(G) The CF of ipsilateral TRF vs. that of contralateral TRF. The black line is the best-fit linear regression line (slope = 0.97). The correlation coefficient r is marked.
(H) An example recording in which both spike and subthreshold responses were observed. Each trace is a 50 ms record. Below, color map on the left represents the spike TRF with the color representing the average spike number, and the map on the right represents the subthreshold TRF. Note that the cell had no ipsilaterally evoked spiking response, but did show ipsilaterally evoked subthreshold responses.

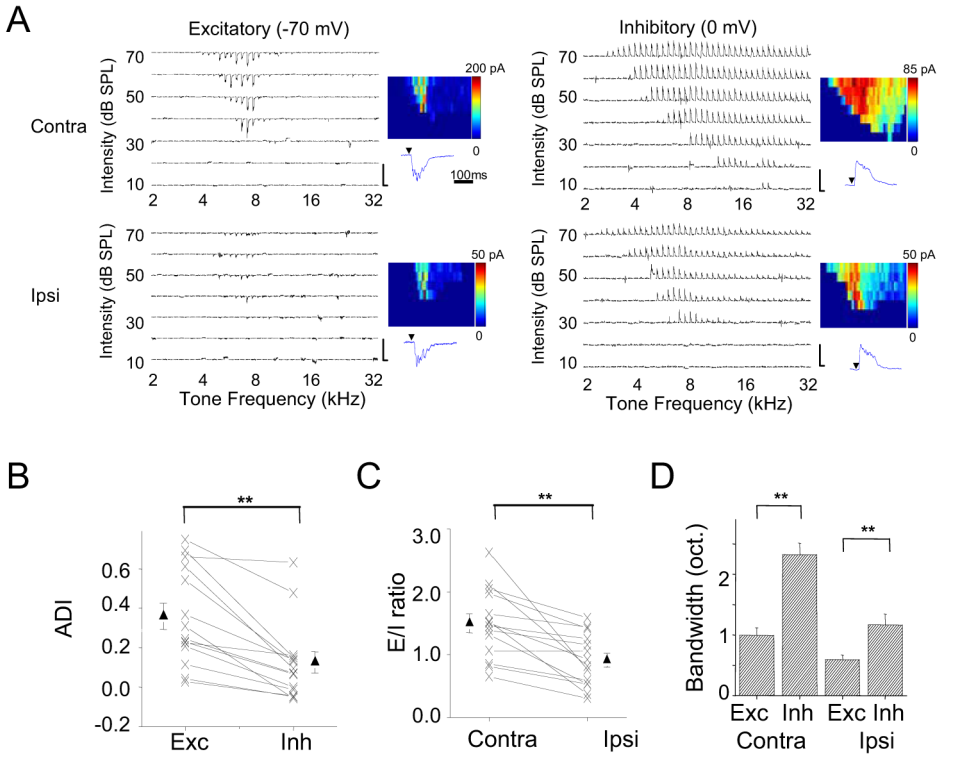

Figure 2. Synaptic inputs underlying the contralateral aural dominance of ICC responses

(A) Whole-cell voltage-clamp recording from an example ICC neuron. Left, TRF of excitatory current recorded at −70 mV. Right, TRF of inhibitory current recorded at 0 mV. Scale, 200 pA, 350 ms. Color map depicts the peak amplitude of synaptic current (averaged for two repetitions). Below the color map is an enlargement of the CF-tone evoked synaptic response (350 ms record). Arrow points to the tone onset.

(B) The measurement of binaural balance for excitation and inhibition with aural dominance index (ADI). Response amplitudes to tones at three frequencies centered on the best frequency and at 70 dB SPL were averaged for this analysis. Data points for the same cell are connected with a line. Solid symbols represent mean ± SEM. **p < 0.001, paired t-test, n = 14. Similar tests and labels apply to (C) and (D).

(C) Excitation/inhibition (E/I) ratio for contralateral and ipsilateral stimulation.

(D) Average bandwidths of excitatory and inhibitory TRFs at 60 dB SPL.

See also Figure S1.

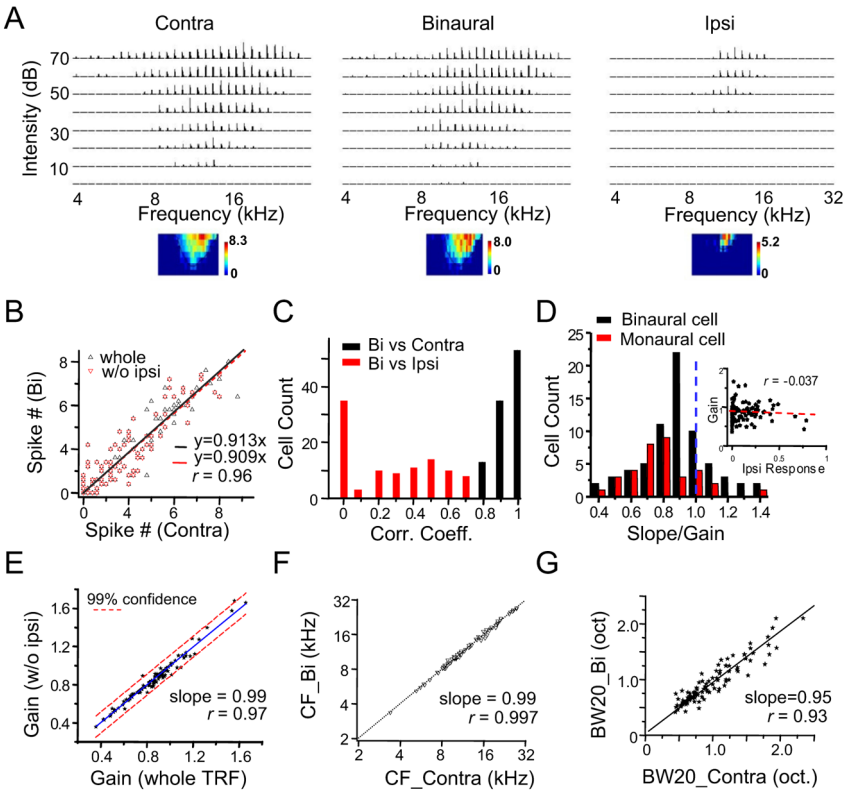

Figure 3. A gain modulation for transforming monaural into binaural response

(A) Contralateral, binaural and ipsilateral spike TRFs of an example ICC neuron. Data presentation is the same as in Figure 1B.

(B) Binaurally evoked spike number vs. contralaterally evoked spike number under the same tone, plotted for the cell shown in (A). Whole (black), responses from the entire TRF; w/o ipsi (red), responses from the TRF region where there were no ipsilateral spiking responses. *r* is 0.96 for both fittings. Bootstrapped slope for the entire TRFis 0.91 ± 0.02 (mean ± SD).

(C) Distribution of correlation coefficients in the recorded population. Bin size = 0.1.

(D) Distribution of gain values. The gain is equivalent to the slope of linear fitting of binaural vs. contralateral response. Black, binaural cells; red, monaural cells. Inset, the gain value plotted as a function of the strength of the ipsilateral response (to CF tone at 60 dB SPL), which is normalized by the strength of the contralateral response.

(E) The gain measured for responses within the effective frequency-intensity region where there were no ipsilateral spiking responses plotted against that measured within the entire TRF. Black line is the best-fit linear regression line. Dash lines mark the 99% confidence interval.

(F) The CF of binaural TRF vs. that of the corresponding contralateral TRF. Dotted line is the best-fit linear regression line.

(G) The bandwidth of binaural TRF vs. that of the corresponding contralateral TRF. Bandwidth was measured at 20 dB above the intensity threshold. Black line is the best-fit linear regression line.

See also Figure S2.

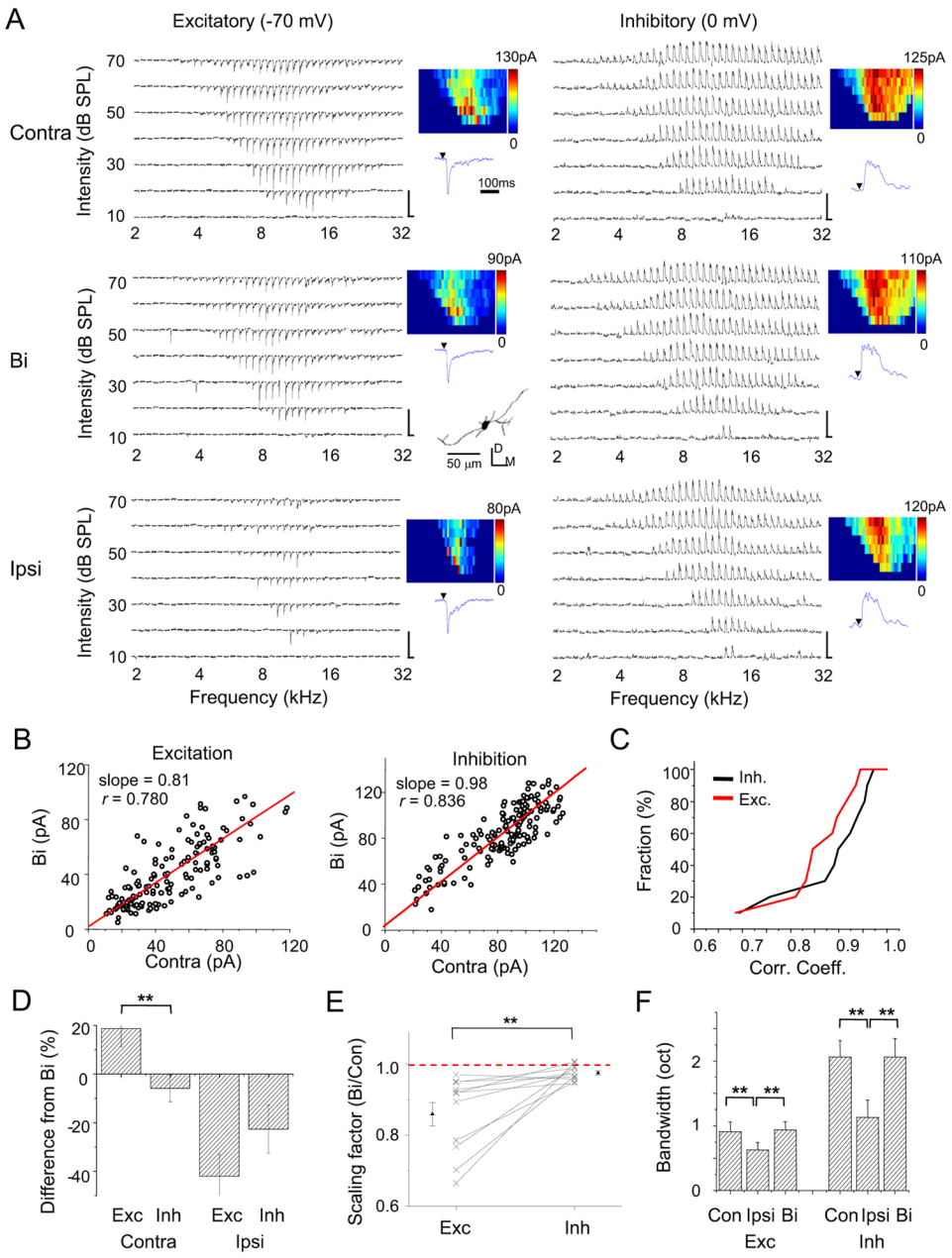

Figure 4. Synaptic inputs underlying binaural interaction

(A) Excitatory and inhibitory synaptic TRFs of an example ICC neuron under contralateral, binaural and ipsilateral stimulation respectively. Data are displayed in the same manner as in Figure 2A. Scale: 150 pA, 350 ms. The reconstructed dendritic morphology of the recorded cell is shown in the middle inset, which is consistent with the reported disc-shaped cell (Oliver et al., 1991). D, dorsal; M, medial.

(B) Binaural synaptic response amplitude vs. the corresponding contralateral response amplitude, plotted for the cell as shown in (A). The best-fit linear regression lines are shown. Slope: 0.81 ± 0.03 for excitation; 0.98 ± 0.01 for inhibition (mean ± SD, bootstrapping).

(C) Accumulative fraction of the correlation coefficient calculated between binaural and contralateral synaptic responses.

(D) Percentage difference of contralateral and ipsilateral response amplitudes from the corresponding binaural response amplitude. Response amplitudes to tones at three frequencies centered on the best frequency and at 70 dB SPL were averaged for this analysis. Bar = SEM. **$p < 0.005$, paired t-test, $n = 11$. Similar tests and labels apply to in (E) and (F).

(E) The overall scaling factor measured for responses within the entire synaptic TRF (Bi vs. Contra). Data points for the same cell are connected with a line.

(F) Average bandwidths synaptic TRFs at 60 dB SPL.

See also Figure S3.

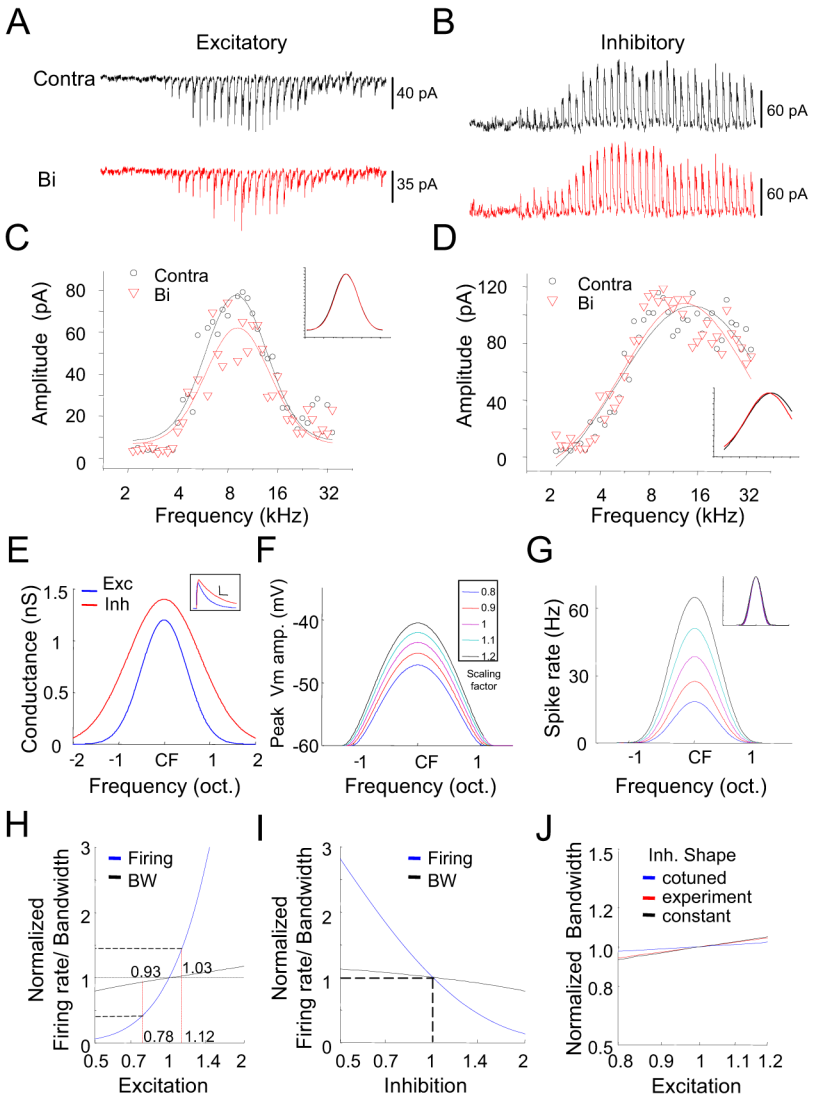

Figure 5. Scaling of excitation can lead to a gain modulation effect

(A and B) An enlargement of tone evoked excitatory (A) and inhibitory (B) responses at 70 dB SPL under contralateral and binaural stimulation. Each small trace (350 ms record) represents the response to a given tone frequency.

(C and D) Plot of the response amplitudes at different frequencies for the same cell. Curves are Gaussian fits of the data. Inset, the Gaussian functions are normalized and superimposed for comparison.

(E) Simulated frequency tuning curves for excitation and inhibition. The tuning curves are centered on the same characteristic frequency. The inhibitory tuning curve is broader than the excitatory tuning curve. Inset, temporal profiles of the simulated tone-evoked excitatory and inhibitory conductances. Scale, 0.5 nS, 40 ms.

(F) Tuning curves of peak membrane depolarization resulting from the integration of the modeled synaptic conductances. Excitatory responses were scaled by a factor of 0.8 – 1.2 while fixing the inhibitory responses. The resting membrane potential is set at −60 mV.

(G) Tuning curves of spike rate under different scaling factors for manipulating excitatory strength. Spike rate was calculated from the peak Vm response based on a power-law function. Inset, spike tuning curves are normalized and superimposed for comparison.

(H) Normalized CF-tone evoked firing rate (blue) and spike tuning width (black) at different scaling factors for scaling excitatory strength. Note that within the physiological range of firing rate changes (0.4–1.4), there is only a very small variation in spike tuning width (0.93–1.03).
(I) Normalized firing rate and spike tuning width at different scaling factors for scaling inhibition (0.5 – 2), with the excitation fixed.
(J) Normalized spike tuning width at different scaling factors for scaling excitation. The inhibitory tuning shape was varied. Cotuned, excitation and inhibition have the same tuning shape; constant, inhibitory tuning is flat.

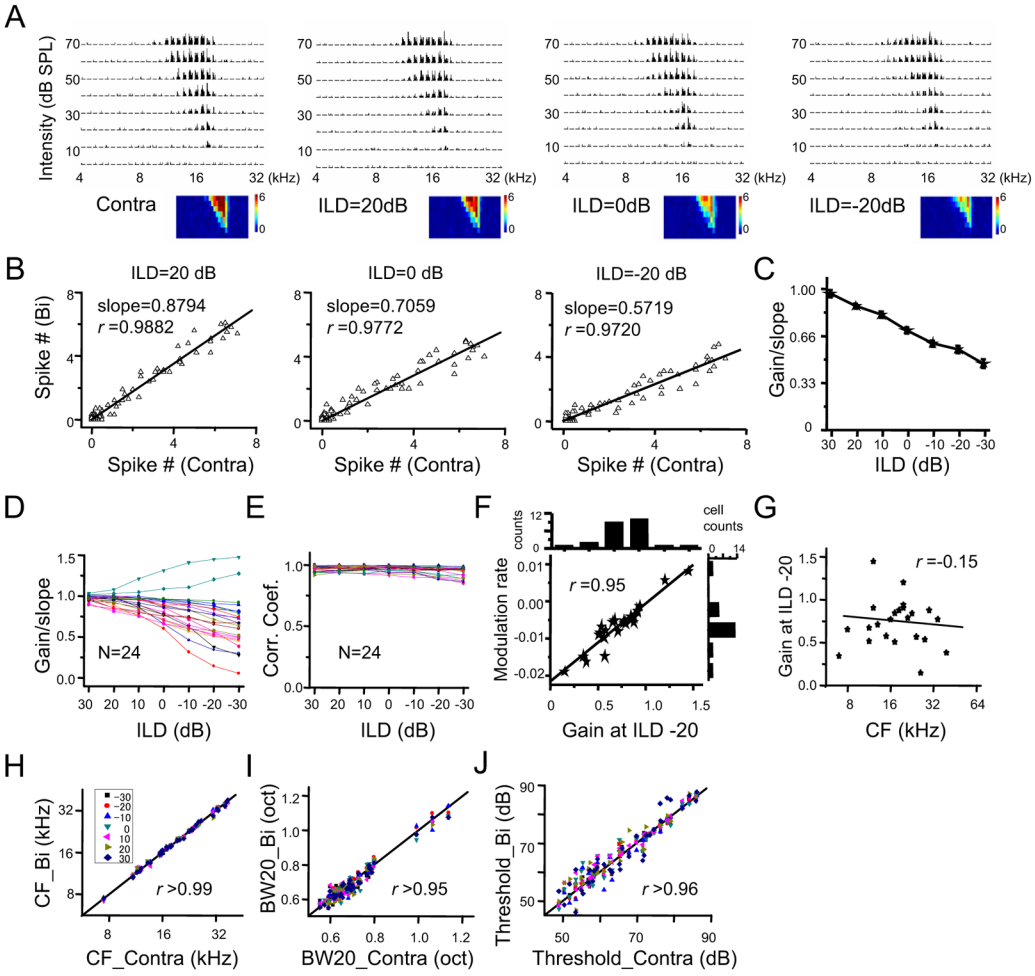

Figure 6. ILD-dependent gain modulation

(A) Contralateral TRF and binaural TRFs at different ILDs of an example ICC neuron. The ILD is presented as contralateral tone intensity – ipsilateral tone intensity.

(B)Plot of binaurally evoked spike number vs. contralaterally evoked spike number for the same cell as shown in (A). The best-fit linear regression lines are shown.

(C) Plot of gain (mean ± SD, 1000 bootstrap samplings) vs. ILD for the same cell as in shown (A).

(D) Plot of the mean of bootstrapped gains at different ILDs for 24 cells recorded. Data from the same cell are connected with a line.

(E) Plot of the correlation coefficient for binaural versus contralateral responses at different ILDs for the same 24 cells.

(F) The rate of modulation versus the gain at −20 dB ILD. The modulation rate is measured by the change of gain from 0 dB to −20 dB ILD divided by 20 dB. Black line is the best-fit linear regression line. The distribution of modulation rates and gains at 20 dB ILD in all the recorded neurons are shown on the top and right respectively.

(G) Plot of gain value (at ILD = −20 dB) versus CF.

(H) CF of binaural TRF vs. CF of the corresponding contralateral TRF at different ILDs (labeled with different colors) for all the recorded cells. Dotted line is the best-fit linear regression line.

(I) Bandwidth of binaural TRF at different ILDs vs. that of the corresponding contralateral TRF. Bandwidth was measured at 20 dB above the intensity threshold.

(J) Intensity threshold of binaural TRF vs. that of the corresponding contralateral TRF. See also Figure S4.

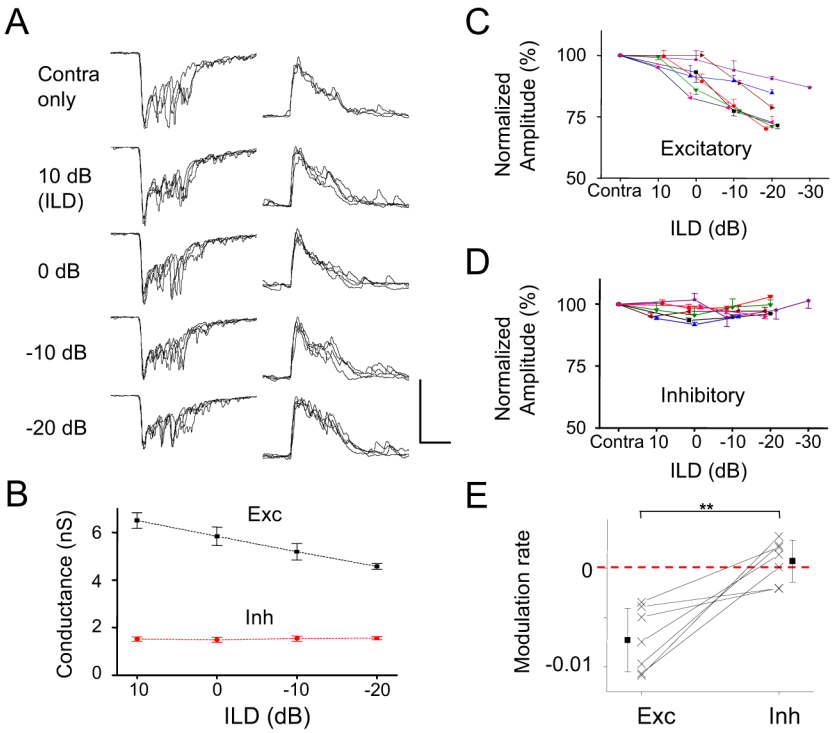

Figure 7. Synaptic responses underlying ILD-dependent gain modulation

(A) Superimposed CF-tone evoked synaptic responses of five repetitions under contralateral stimulation only and binaural stimulation at different ILDs in an example cell. Scale: 450 pA (left)/100 pA (right), 50 ms.

(B) The mean ± SD of peak synaptic response amplitude at different ILDs for the cell shown in (A).

(C) The mean ± SD of peak excitatory response amplitudes for contralateral stimulation and binaural stimulation at different ILDs in seven cells. Each color represents one individual cell.

(D) The mean ± SD of peak inhibitory response amplitudes for the same seven cells.

(E) The rate of modulation (/dB). It is calculated by subtracting the level of binaural response at ILD = 0 dB from that at ILD = −20 dB, then divided by 20. Solid symbols represent mean ± SD. **p < 0.01, paired t-test.

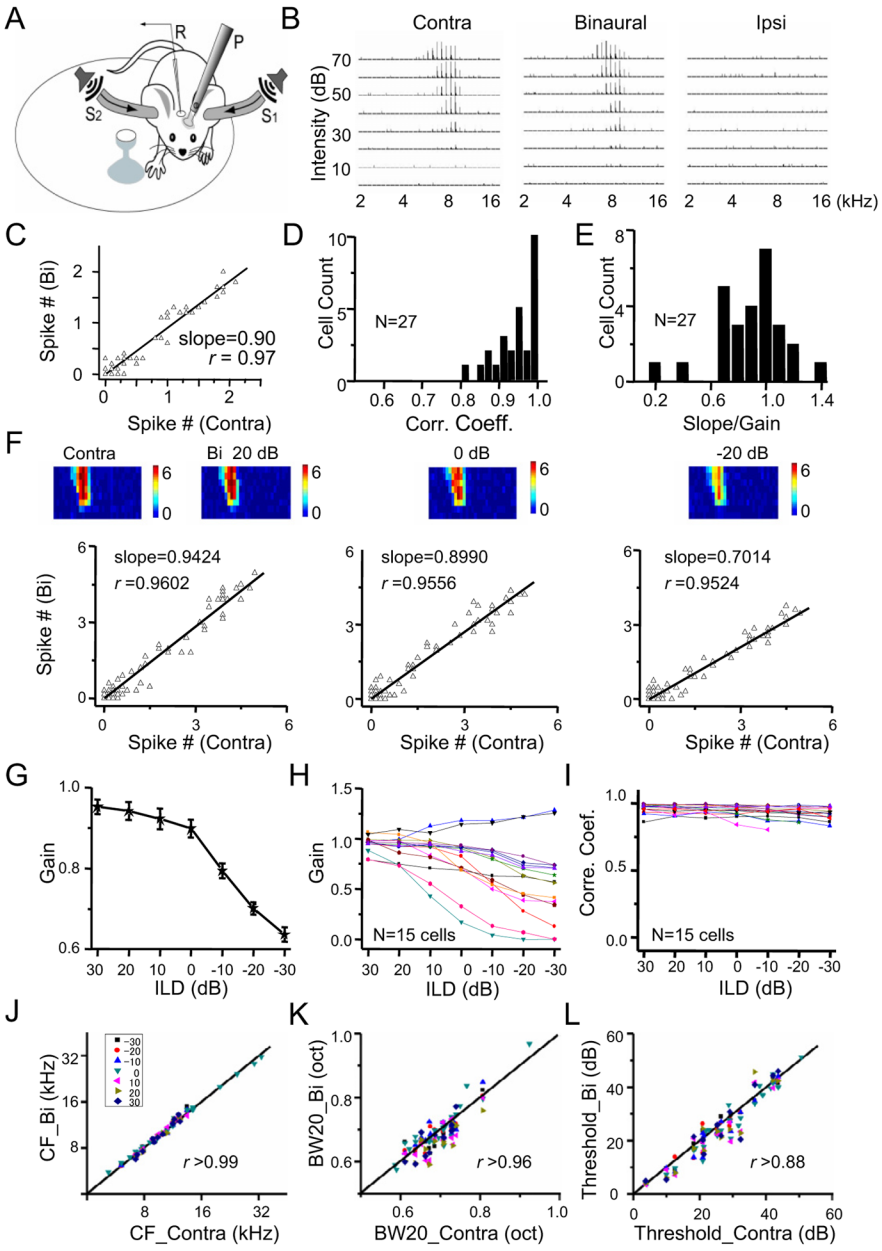

Figure 8. Binaural interaction in the awake ICC

(A) A schematic drawing of our awake recording setup. R, recording electrode. P, metal post for head fixation. S, tube for enclosed sound delivery, which is coupled to a speaker. The mouse is allowed to run freely on a rotatable plate.

(B)Contralateral, binaural (ILD = 0 dB), and ipsilateral spike TRFs of an example neuron in the awake ICC. Data presentation is the same as in Figure 1B.

(C) Plot of binaurally evoked spike number vs. the contralaterally evoked spike number for the cell shown in (B).

(D) Distribution of the correlation coefficient for binaural (at ILD = 0 dB) versus contralateral responses. N =27 cells.

(E) Distribution of the mean of bootstrapped gain values. N =27 cells.

(F) Contralateral TRF and binaural TRFs at different ILDs of another example cell. Top, color map depicts the average evoked spike number per stimulus. Bottom, plot of binaurally evoked spike number vs. contralaterally evoked spike number for the corresponding hearing condition.
(G) The mean ± SD of bootstrapped gain values at different ILDs for the cell shown in (F).
(H) The mean of bootstrapped gain values at different ILDs plotted for 15 recorded cells.
(I) Plot of correlation coefficients at different ILDs for 15 recorded cells.
(J–L) Comparison of CF (J), tuning bandwidth (K) and intensity threshold (L) between binaural and contralateral TRFs.